

Briquetting of waste glass cullet fine particles for energy-saving glass manufacture

DENG, Wei, WRIGHT, Richard, BODEN-HOOK, Chris and BINGHAM, Paul
<<http://orcid.org/0000-0001-6017-0798>>

Available from Sheffield Hallam University Research Archive (SHURA) at:

<https://shura.shu.ac.uk/18808/>

This document is the Accepted Version [AM]

Citation:

DENG, Wei, WRIGHT, Richard, BODEN-HOOK, Chris and BINGHAM, Paul (2018).
Briquetting of waste glass cullet fine particles for energy-saving glass manufacture.
Glass Technology: European Journal of Glass Science and Technology Part A, 59
(3), 81-91. [Article]

Copyright and re-use policy

See <http://shura.shu.ac.uk/information.html>

1 **Briquetting of waste glass cullet fine particles for energy-saving glass**
2 **manufacture**

3 **Wei Deng ^a, Richard Wright ^b, Chris Boden-Hook ^b and Paul A Bingham ^{a,1}**

4 ^a. Materials and Engineering Research Institute, Faculty of Arts, Computing, Engineering and
5 Sciences, Sheffield Hallam University, City Campus, Howard Street, Sheffield S1 1WB, UK

6 ^b. Wright Engineering Ltd, Blyth Road, Worksop S81 8BP, UK

7 **Abstract**

8 Fine particles of glass cullet (fines) arising during glass recycling cannot presently
9 be recycled into glass manufacture due to the potential for bubble formation and
10 foaming. Consolidation of glass fines into briquettes could enable their
11 re-introduction into furnaces, reducing waste and glass melting energies. Properties of
12 briquetted cullet fines and briquette melting behaviour in soda-lime-silica glass
13 batches are presented. Morphology and density of glass fines and briquettes; and
14 briquette mass and mechanical properties as functions of time after formation were
15 analyzed. Compressive strength increases linearly with time after briquette formation.
16 With slight batch modifications to maintain the same final glass composition, up to 15
17 wt % briquettes were successfully added to a representative container glass batch and
18 melted. Results confirm that briquette batch additions can provide equivalent final
19 glass composition, optical absorption characteristics and redox to briquette-free
20 batches, supporting their industrial uptake.

21 **Keywords:** glass; cullet; energy; emissions; briquette; consolidation

¹ Corresponding author, email p.a.bingham@shu.ac.uk

22 **1. Introduction**

23 It is well known that the introduction of recycled glass (cullet) into commercial
24 industrial glass batches can significantly reduce glass melting energy requirements
25 and CO₂ emissions.[1-3] Cullet can act as a fluxing agent and decreases the glass
26 melting energy and thus Specific Energy Consumption (SEC). Compared to virgin
27 (mined and man-made) glass batch raw materials, the melting energy consumption of
28 cullet is approximately 70-75 % [4]. However, collection, recycling and transportation
29 of cullet produces a significant fraction of fine particles which cannot be directly
30 re-introduced into glass furnaces and are thus currently treated as a waste and
31 discarded. The glass industry has strict requirements for the particle size distribution
32 of batch components [5]. Specifically, very small particles (typically 6mm diameter or
33 less and cannot be sorted using existing optical technology) of glass cullet or batch
34 raw materials can cause dust formation prior to and after entry to the furnace [5];
35 entrainment of many tiny bubbles or “seed” in the glass melt; and foaming of the melt
36 in furnace [6]. Moreover, fine particles can have both corrosive and erosive effects on
37 furnace refractories [6, 7] and they can block or foul the checkers in furnace
38 regenerators [7]. Typically 20% of recycled cullet is rejected on account of its fine
39 particle size, and in the UK most of this is currently sent to landfill [8] or into
40 aggregates. If the rejected cullet fines can be reclaimed or consolidated in such a way
41 that they can be re-melted as glass batch constituents, the growing shortages of
42 landfill sites and high-quality recycled cullet for glass manufacture could be alleviated,
43 whilst at the same time replacing virgin (mined) raw materials, reducing batch CO₂

44 emissions, and reducing the SEC of glass manufacture (and therefore fuel CO₂
45 emissions as most glass furnaces are gas-fired).

46 In the present study a briquetting technology, utilizing a novel binder has been
47 applied to the problem of glass cullet fines, with the aim of enabling their recycling
48 and re-melting in industrial glass manufacture. The research described in this paper is
49 the result of an ongoing project with the aim of gaining a clearer understanding of the
50 effects of introducing briquetted glass fines into full-scale glass manufacture in terms
51 of melting rates, refining, redox, colour and energy saving.

52 In addition to controlling the particle size distribution, granulation of virgin glass
53 batch raw materials to avoid dust formation and evolution during melting has
54 previously been attempted [9]. More widely, granulation (very small, < ca. 10 mm
55 diameter), pelletisation (small, < ca. 20 mm diameter) and briquetting (larger, < ca. 50
56 mm diameter) processes have all been researched in the glass industry [9-11].
57 However, these methods have hitherto been applied only to virgin glass batch
58 materials (i.e. sand, sodium carbonate, limestone, dolomite, etc.) and not to glass
59 cullet fines [9, 11]. Different inorganic and organic chemicals and minerals have been
60 considered as binder materials in the production of consolidated glass batches. These
61 binders have included paper pulp, cellulose, bentonite and carbonates [12, 13].
62 Potentially, briquetting can give greater advantages in terms of formation and strength
63 than pelletisation or granulation, since briquettes are formed with the application of
64 external pressure, whereas granules and pellets are gravity-formed with no external
65 pressure applied. Consequently, granules and pellets exhibit greater friability and

66 lower mechanical strength and cohesion. Consolidated batch and / or cullet can also
67 provide advantages in the furnace such as decreased melting and refining times [5, 9,
68 13], increased batch thermal conductivity compared with unconsolidated batch
69 materials, shorter batch blankets on the surface of the melt [9] and higher output of
70 glass or “pull rate” [14]. All of these can contribute to lower SEC and fuel
71 consumption and hence lower CO₂ emissions from glass manufacture.

72 As a reusable raw material, glass fines will have their own characteristic effects
73 on the final glass quality. Bulk glass cullet can have a moderately reducing effect on
74 redox conditions during melting due to organic contamination such as residual
75 foodstuffs, labels and glue, particularly from cullet collected from public bottle banks.
76 This reductive contamination affects the partial pressure of oxygen (pO_2) in and above
77 the glass melt in the furnace, and can in some circumstances lead to problems with
78 final glass colour and refining. Most importantly, glass colour will be affected, as the
79 Fe^{2+}/Fe^{3+} ratio varies with pO_2 [15] and under strongly reducing conditions the
80 well-known $Fe^{3+}-S^{2-}$ amber chromophore can form [16-18]. Under less reducing
81 conditions than those required to form full amber colour, an olive-green colour can
82 form [17, 18]. Such colours may be undesirable if the aim is to manufacture a
83 colourless or green glass. To provide the correct redox balance, oxidizing agents such
84 as sulphates, nitrates and oxides of manganese, cerium, arsenic or antimony can be
85 added to the batch [16-19]. However, a preferable solution is to control the levels of
86 organic cullet contamination, rather than attempt to offset its effects through adding
87 other dopants or oxidizing agents. Compared to bulk cullet, the specific surface area

88 of glass fines is relatively high and coupled with this, glass fines contain more
89 contamination such as ceramics and organics. Modifying the batch to adapt to these
90 effects, if necessary, is thus a consideration.

91 In this study, briquetted glass fines were manufactured and tested. A mixture of
92 glass fines with appropriate additions of a binder material and water was formed as
93 briquettes using the application of a mould and pressure. The density, compressive
94 strength and weight loss of the resulting briquettes were investigated as a function of
95 time after briquette formation. For comparative glass melting and property
96 assessments, a representative green container glass batch with 87 wt % cullet was
97 chosen as a benchmark. With compensation of the batch to maintain the same final
98 glass composition with and without briquette additions, glass batches containing
99 different amounts of briquettes were melted, wherein the briquettes partially replaced
100 the regular cullet so as to maintain the same overall recycled glass (briquettes + cullet)
101 percentage. UV-Vis-IR absorption spectroscopy was used to determine the optical
102 absorption spectra, and hence the colour and redox ($\text{Fe}^{2+}/\Sigma\text{Fe}$) ratio estimation of all
103 glasses.

104 **2. Experimental Procedures**

105 Glass fines, which were originally destined to be sent to landfill, were collected
106 from a German recycled glass supplier. An Olympus BX 51 optical microscope was
107 used to characterize the appearance and constituents (amber, green or colourless glass;
108 ceramics, organics) of received glass fines, prior to briquetting. To enable comparison
109 of as-received glass fines with clean fines, the as-received glass fines were cleaned

110 using acetone in an ultrasonic bath for 2 minutes. Very thin specimens (about 2mm
111 thick) were prepared for optical microscope. The sieving method was used for glass
112 fines particle sizes distribution measurement, and the particle sizes of the glass fines
113 are given in Figure 1.

114 Briquettes were manufactured by mixing sodium silicate ($\text{Na}_2\text{O}\cdot 2\text{SiO}_2$), sodium
115 carbonate (Na_2CO_3), glass fines and water. Briquettes were produced using a
116 proprietary mechanical mixing and forming method which consistently produced
117 briquettes of typical dimensions 20 x 30 x 40 mm. After thorough mixing of the
118 briquette constituents, the mixture was fed into a roller press with moulds on a double
119 roll to compress the mixture into a briquette at applied pressures of approx, 50 MPa.
120 After formation, briquettes then passed along a conveyor belt with heating to partially
121 dry them, and after 2 minutes were deposited from the end of the conveyor into large
122 bags. Briquettes were then collected for analysis.

123 Measured densities of briquettes, glass and glass fines are shown in Table 2. The
124 bulk density of glass fines was measured 3 times for each sample using a standard
125 density apparatus according to BS EN 459-2:2010. The true density of container glass
126 cullet and glass fines have been measured by the Archimedes method using distilled
127 water as the suspension medium. Densities were calculated using (1):

128

$$129 \quad \rho = \left[\frac{W_A}{W_A - W_W} \right] \delta_w \quad (1)$$

130

131 where ρ = density in g cm^{-3} ; W_A = weight in air; W_W = weight in water and δ_w = water

132 density with temperature correction. Bulk density of briquettes was measured by the
133 Archimedes method. To prevent interactions with the measurement medium (water),
134 samples were embedded in paraffin. Briquette densities were calculated using (2):

$$\rho_B = \frac{W_B}{\left[\left(\frac{W_A}{\rho_A} \right) - \left(\frac{W_p}{\rho_p} \right) \right]} \quad (2)$$

136

137 where ρ_B = density of briquette in g cm^{-3} ; W_B = weight of briquette in air; W_A = weight
138 of paraffin-embedded briquette in air; ρ_A = density of paraffin-embedded briquette,
139 which can be calculated by Archimedes method; W_p = weight of paraffin, which is the
140 weight difference before and after the embedded process and ρ_p = density of paraffin.

141 Weight loss as a function of time after manufacture was measured for 20 briquettes at
142 room temperature (ca. 20 °C) using a high-precision 2 decimal place balance. The
143 results are shown in Figure 4. Under identical conditions, the compressive strength of
144 briquettes was measured using an INSTRON 2530-445 (capacity: 50kN) as a function
145 of time since briquette formation, the values provided here being determined as
146 averages value of at least 3 measurements. Results are shown in Figure 5. To
147 characterize the morphology, microstructure and composition of briquettes, samples
148 were coated by ~20 nm carbon film for SEM (FEI Quanta 650) and EDS (Oxford
149 Instruments/line scan mode) characterization.

150 The representative (benchmark) green container glass batch and modified batches
151 containing briquettes replacing standard cullet that were melted under laboratory
152 conditions, are presented in Table 3. Series One batches were produced, wherein

153 briquettes partially replaced standard cullet at several levels from 0 to 20 wt %.
154 Sample naming is of the form B-#, where # denotes the amount of briquettes added in
155 weight %. Series Two batches were variants of the Series One B-15 batch, wherein
156 the levels of added colourants were varied in order to provide colouration comparable
157 to the benchmark glass. These samples are denoted B-15a, b, c and d. In addition,
158 samples of as-received glass fines, briquettes and general glass cullet were each
159 re-melted to enable comparative optical absorption measurements. Industrial raw
160 materials and cullet were obtained from a UK container glass manufacturer, and
161 batches were weighed out using a 2 decimal place balance to provide batches
162 weighing 200g. Batches were thoroughly mixed and were then placed in recrystallized
163 Al₂O₃ crucibles. Crucibles were heated in an electric furnace at a rate of 4°C / minute
164 to 1450°C and then held at this temperature for 4h. Crucibles were then removed from
165 the furnace and the molten glass poured into a stainless steel mould and allowed to
166 cool until sufficiently rigid to remove the mould. The glass was then annealed at
167 520°C for 1h, then cooled slowly to room temperature. Resulting glass compositions
168 were determined using X-ray fluorescence spectroscopy (wavelength dispersive
169 Philips PW2440 sequential X-ray fluorescence spectrometer) and results are presented
170 in Table 3. Uncertainties associated with the XRF analyses are estimated at ±2% of
171 measured concentrations.

172 Glass samples were prepared for optical spectroscopy measurement by grinding
173 using successively finer SiC grinding pads from 60 to 1200 grit size, then polished
174 using a suspension of CeO₂ powder in water to provide a highly polished (< 1µm)

175 surface finish. Optical absorption spectra were measured using a Varian 50Scan
176 UV-Visible-near-IR spectrophotometer over the wavelength range 300-1000 nm. The
177 repeatability of measured absorbance data was confirmed by measuring each sample 3
178 times.

179

180 **3. Results**

181 The glass batch compositions used in this research are given in Table 1 (a) and (b).
182 Owing to the presence of binder materials in briquettes, and in order to keep the final
183 target glass composition unchanged, briquette-containing glass batches were modified
184 slightly. For Series One batches, sample B-15 is close to the upper limit for achieving
185 an unchanged nominal final glass composition, whilst sample B-20X presents a
186 slightly elevated Na₂O content in the final glass, despite removing all Na₂CO₃ from
187 the raw materials, due to the binders present in the briquettes used. Series Two
188 batches B-15a, b, c, d, with modification of colourant and oxidant constituents are
189 shown in Table 1 (b). Manganese ore and chromite contents were varied. XRF
190 analyses of final glasses are shown in Table 2. This confirms, within experimental
191 uncertainties, that the chemical composition of the benchmark glass was largely
192 maintained for B-9 and B-15 glasses, however, small increases in SiO₂ content are
193 likely to have resulted from corresponding small differences in SiO₂ and CaO content
194 of glass fines compared with cullet. Further batch modification would be required to
195 fine-tune this, for example by slightly increasing the limestone contents of
196 briquette-containing batches. Such modifications are regularly carried out in the glass

197 industry.

198 The particle size distribution (PSD) of the glass fines is given in Figure 1. There were
199 no particles larger than 2 mm diameter; 37.8 wt % were between 0.5 and 2 mm; 46.8
200 wt % between 0.25 and 0.5 mm; 11 wt % between 0.125 and 0.25 mm; 3.2 wt %
201 between 0.125 and 0.062 mm, and the balance (1.6 wt%) smaller than 0.062mm.

202 Figure 2 shows optical micrographs of glass fines before and after cleaning in acetone.
203 Under optical microscopy, fines are shown to be a mixture of amber, flint and green
204 glass particles. For the as-received samples, considerable levels of contaminants are
205 observed. A simple loss-on-ignition (LOI) analysis of raw glass fines was carried out
206 by heating 10 g of glass fines at 100 °C and 700 °C each for 3h, and showed a
207 moisture loss of 0.13 ± 0.04 wt % at 100°C and a total weight loss of 0.75 ± 0.07 wt%
208 at 700°C. Considering their relatively low density, these organic contaminants impact
209 on redox and are discussed in Section 4. The optical and secondary electron SEM
210 micrographs of briquette cross-sections are presented in Fig. 3a and Fig. 3b.
211 Briquettes exhibit a dense and compact microstructure. The EDS line scan shows a
212 continuous phase - glass particle interface in briquettes (Fig. 3c and 3d).

213 Note from Richard. Should we mention something here about the fines needing to be
214 at 1 mm or less because of CSP inclusions. During residence time in glass melting
215 these can dilute into the bath causing no reduction in final quality

216 The bulk and true densities of standard cullet, glass fines and briquettes are shown in
217 Table 3. The true density of glass fines (2.513 g/cm^3) is close to that of standard cullet
218 (2.544 g/cm^3), as would be expected. For the porous and powder form, glass fines

219 contain a lot of air, the bulk density of glass fines is, however, very low as would be
220 expected. Yet bulk density increased from 1.311 to 2.105 g/cm³ after briquetting. This
221 is consistent with the optical microscopy results in Fig. 2, which confirm that the
222 contact area of glass fines in briquettes is greatly increased, and thus the voids /
223 porosity are substantially decreased. This suggests that thermal conductivity of
224 briquettes should be substantially greater than unconsolidated glass fines. The thermal
225 conductivity of glass batch was measured over the range 100°C to 1250°C by Kröger
226 and Eligehausen [20]. More recently, further data on thermal conductivity of glass
227 batches were reported by Verheijen *et al.* [21], Schill [22] and Hrma *et al.* [23]. Their
228 studies focused on the precise measurement of effective thermal conductivities in
229 different glass batches. A gradually linear increase of thermal conductivity was
230 observed from ~100°C to ~650°C, before a sudden rapid increase above 700~750°C
231 which may be due to liquid phase formation [21, 23]. The thermal conductivity of
232 loose (unconsolidated) glass batch at room temperature is 0.273 W/m·°C. It was
233 increased to 0.430 W/m·°C as the bulk density increased from 1.291 g/cm³ to 2.124
234 g/cm³ by compression (consolidation) of the batch [24]. Meanwhile, the thermal
235 diffusivity of cullet is always higher than that of virgin glass batch during heating [25].
236 Thus, as a consolidation method, briquetting of glass fines can provide a net increase
237 in thermal conductivity compared with loose glass fines.

238 In Figure 4, weight loss curves of 20 briquettes at room temperature are presented.
239 They show that, although the briquettes have the same nominal composition and are
240 produced under essentially the same conditions, weight loss rates vary somewhat for

241 different briquettes.

242 Figure 5 shows the measured compressive strength of briquettes as a function of
243 time from formation. The initial strength of briquettes is relatively low and not more
244 than 5 MPa in the first 5 days, rising to ~60 MPa after 30 days.

245 UV-Vis-IR absorption spectra of benchmark glass, melted glass fines, melted
246 briquettes and melted standard cullet within the wavelength range of 300-1000 nm are
247 presented in Figure 6a. For every curve, the UV absorption edge is near 370 nm, and
248 spectra contain one narrow absorption band at 380 nm and two wider absorption
249 bands centered at ca. 450 nm and 660 – 700 nm. Compared to the benchmark glass,
250 the absorbance of melted glass fines, briquettes and standard cullet in the visible
251 region (ca. 400 – 650 nm) is lower. A broad optical absorption band centered at a
252 wavelength of ~1100 nm was also observed in melted glass fines, melted briquette
253 and melted general cullet samples. As shown in Figure 6b, the absorption spectrum of
254 samples B-0, B-9, B-15 and B-20X are almost the same. In Figure 6c, the absorption
255 spectra of samples B-15a, b, c and d, produced with varying amount of manganese ore
256 and chrome premix additions, are presented. The strength of the absorption bands
257 centered at 450 nm and 660-700 nm in samples B-15a and B-15b are lower than that
258 of sample B-15, and the broad absorption band centered at ~1100 nm in sample B-15a
259 is present. Meanwhile, the absorption spectrum of sample B-15c is similar to sample
260 B-15 at < 700 nm, however, at wavelengths above 700 nm, the absorption strength of
261 sample B-15c increases. For the sample B-15d spectrum, the absorbance below ~700
262 nm is relatively low and above 700 nm it is relatively high compared to sample B-15.

263

264 **4. Discussion**

265 **4.1. Briquettes**

266 As described in Sections 1 and 2, a small particle size is the biggest obstacle for
267 the recycling of glass cullet fines into glass furnaces. A screen classification method
268 was used to investigate the particle size distribution of the glass fines studied here.
269 From Figure 1, the particle size distribution of glass fines is not a normal distribution:
270 this can be explained because larger particles are routinely separated and extracted by
271 cullet suppliers. No particle is larger than 2mm. These glass fines will carry entrained
272 air into the glass furnace and hence into the melt, not only increasing furnace dusting
273 [5] and reducing the thermal conductivity of the batch blanket [5], but also causing
274 melt foaming and making satisfactory melt refining more difficult [5-7].

275 As a glass batch raw material, the components of glass fines need to be
276 understood. For standard bulk glass cullet, the proportions of amber, green and
277 colourless cullet and organic contamination can now be closely controlled [9]. The
278 chemical composition of different colours of bulk cullet is similar, except for the
279 colorants and, in certain cases, SO_3 contents. To investigate cullet composition, we
280 re-melted standard bulk cullet and compared it with re-melted glass fines using XRF.
281 As shown in Table 3, XRF analyses of remelted cullet and remelted glass fines are
282 similar, especially for colouring agents Cr_2O_3 , MnO and Fe_2O_3 . This supports the
283 view that re-introduction of glass fines into glass batches can be achieved without the
284 need for substantial modification of batch composition.

285 In Figure 2, the morphology of glass fines, studied by optical microscopy, is
286 demonstrated. For the raw glass fines in Fig.2a, ultra-fine particles and contaminants
287 also accompany the glass fines. The ultra-fine particles cause dispersion and make the
288 luminous environment, observed under white light, complex. However, it is still
289 possible to distinguish individual amber, green and colourless glass fine particles.
290 After washing in acetone, the cleaned glass fines are presented in Fig.2b. The ultrafine
291 particles and contaminants have been removed and very clean glass particles can be
292 observed, again highlighting the presence of colourless, green and amber glass
293 particles. This is expected at some level for all bottle bank cullet, which may be sorted
294 or unsorted by colour.

295 From Table 3, the bulk density of briquettes is obviously higher than that of glass
296 fines and close to the real density of bulk glass. The compressive process of briquette
297 manufacture removes voids and entrained air between glass particles effectively and
298 also introduces the binder constituents into some of the existing void space. The
299 briquette cross-section is characterized by optical microscopy and SEM in Fig. 3a and
300 3b. Glass fine particles are encased in a continuous, dense structure, with binder
301 materials effectively holding the fine glass particles together whilst removing porosity.
302 To demonstrate the interface between the binder phase and glass particles, an SEM
303 image is shown in Fig. 3c. An EDS line scan was performed and the quantitative
304 result is shown in Fig. 3d. The Na and C contents in the binder phase are higher than
305 the surrounding glass fines; and the Si content is higher in the glass fines than in the
306 binder phase. This is fully consistent with the binder phase ingredients ($\text{Na}_2\text{O} \cdot 2\text{SiO}_2$

307 and Na₂CO₃). There is no evidence of extensive chemical interaction between binder
308 and glass fines phases, however, the “pore-filling” action of the binder phase can be
309 clearly seen.

310 It has long been known that sodium silicate can be used in sand casting processes
311 as a highly effective inorganic binder to provide high strength performance [26, 27].
312 Here, briquettes required a binder that provide this function but also require strength
313 after forming to enable problem-free transport into the furnace without fragmentation
314 or excessive friability. Thus, sodium silicate was introduced as binder component here.
315 Theoretically, the chemical reaction of sodium silicate-bonded, CO₂ hardened sand
316 system, or the so called “silicate-CO₂ process” [27] can be expressed as (3):

317



319

320 The formation of amorphous silica gel from sodium silicate as in (3) requires
321 water and CO₂ from air, but also time for solidification. As a batch component here,
322 water was introduced into the briquetting process to improve the rheology of glass
323 fines and binder mixtures during the briquetting process. However, too much residual
324 water may delay the solidification time, reduce the strength, or even make the
325 briquette thixotropic. Therefore it had to be carefully controlled to ensure
326 problem-free briquette manufacture.

327 Figure 4 shows the weight loss of 20 briquettes as a function of time after
328 formation, to understand drying and hydration reactions with time. After storage at

329 room temperature (ca. 20 °C) for approximately 150 hours, weight loss reaches a
330 steady state and further weight loss becomes very slow. In Fig.7 a), the instant weight
331 loss rates (R_I) of different briquettes are presented and calculated with weight
332 difference between adjacent measurements divided by time. The initial rates are
333 relatively fast in the first 75 hours, then the loss rates fluctuate around +/-0.005 wt% /
334 h. Interestingly, some variability is observed in weight loss curves for different
335 briquettes. In Fig.7 b), the average weight loss rates (R_a) of 20 briquettes after 187
336 hours are demonstrated as the function of briquettes initial weight, and calculated with
337 weight difference between the current and initial measurement divided by the time.
338 Weight loss rates decreased with increasing of initial weight. This shows that water
339 removal from a heavy briquette is slower than for a lighter briquette. Briquette sizes
340 did vary, owing to the method of formation, with some being thicker and others
341 thinner. This result strongly suggests that weight loss differences are due to
342 differences in surface area to volume (SA/V) ratio, i.e. lighter briquettes have a larger
343 SA/V ratio and therefore water removal (drying) is more rapid compared to heavier
344 briquettes. In Fig.7 c), the relationships between initial weight of briquettes and
345 average weight loss rate at different time are presented. The average weight loss rates
346 are similar to one another and the influence of initial weight on the weight loss rate is
347 gradually reduced. Clearly water evaporation plays a primary role on the weight loss
348 during this period. However, the reaction of sodium silicate in the binder with CO₂
349 from air, carbonation [27], also needs to be considered because this process will
350 slightly increase the weight of briquette.

351 Compressive strength of briquettes increases linearly as a function of time after
352 formation, as shown in Figure 5. The carbonation of sodium silicate needs time to
353 form silica gel similarly to hydration of concrete from a dynamic viewpoint [28].

354

355 **4.2. Composition, colour and redox of glass**

356 Since the composition of recycled glass cullet is similar to the composition of the
357 glass fines (Table 3b), briquettes can be added into the batch whilst changes in the
358 accompanying glass batch can compensate for the extra Na_2O and SiO_2 arising from
359 the binders. With precise design, the chemical composition of Base line, B-9 and B-15
360 glasses are closely similar, with those differences that do arise being attributable to
361 cullet and glass fines impurities and compositional differences, and to uncertainties
362 associated with the XRF analyses. For sample B-20X, it was not possible to fully
363 balance the additional Na_2O and Na_2CO_3 from the briquette binder by removing batch
364 Na_2CO_3 , and consequently the Na_2O content of this glass is higher than the
365 benchmark. However, the other ingredients in B-20X are as same as in the Base Line
366 sample.

367 As described in Section 1, batch redox plays an important role in glass
368 manufacture, particularly in the preparation of homogeneous glass free from bubbles
369 and in making colored glasses containing transition metal ions [29]. For some
370 transition metal ions UV-Vis absorption spectra can not only characterize the colour
371 properties of glass in the visible light region, but also the redox of different glasses
372 can be deduced and compared from the relative intensity of optical absorption spectra.

373 It is well known that glass redox status can be estimated through the $\text{Fe}^{2+}/\text{Fe}^{3+}$ or
374 $\text{Fe}^{2+}/\Sigma\text{Fe}$ ratio [30-32]. As a colourant ion, Fe^{2+} gives a stronger blue colour in silicate
375 glass whilst Fe^{3+} gives a weaker yellow-green colour [33]. The $\text{Fe}^{2+}/\Sigma\text{Fe}$ ratio gives an
376 indication of the oxidation state of the glass [15]. According to ligand field theory, the
377 absorbance peaks due to $d-d$ transitions of Fe^{2+} and Fe^{3+} were summarized previously
378 [30, 34]. In Fig.6 a), the absorption spectra of Base Line, remelted briquette, remelted
379 cullet and remelted glass fines samples are presented. The optical absorption band
380 centred at ~ 380 nm is attributable to the ${}^6\text{A}_1(\text{S}) \rightarrow {}^4\text{E}(\text{D})$ transition of tetrahedrally
381 coordinated Fe^{3+} cations. The intensity of this band is positively associated with the
382 concentration of Fe^{3+} . For remelted briquette, cullet and glass fine samples, a broad
383 optical absorption band centered at a wavelength of slightly higher than 1000 nm is
384 attributable to the ${}^5\text{A}_2(\text{S}) \rightarrow {}^5\text{E}(\text{D})$ transition of octahedrally coordinated Fe^{2+} cations.
385 The increase in intensity of this band for the remelted briquette, cullet and glass fines
386 samples compared with the Base Line glass, coupled with the opposing trend of
387 decreasing intensity of the Fe^{3+} band at 380nm, confirms that the $\text{Fe}^{2+}/\Sigma\text{Fe}$ ratio is
388 higher in the remelted briquette, cullet and cullet fines samples than the Base Line
389 glass. In the UV edge part of spectrum, there are strong UV peaks from Fe^{2+} (centered
390 ~ 214 nm) and Fe^{3+} (centered ~ 254 nm), which are caused by the charge transfer of 3d
391 to 4s[30]. The UV edge intensity increases and moves towards longer wavelengths
392 with decreasing $\text{Fe}^{2+}/\Sigma\text{Fe}$ ratio, i.e. with increasing oxidation of the melt. Organic
393 contamination in recycled cullet or glass fines shifts the redox equilibrium $\text{Fe}^{2+} \leftrightarrow$
394 Fe^{3+} to the left in the glass melting furnace, increasing the $\text{Fe}^{2+}/\Sigma\text{Fe}$ ratio.

395 For chromium, Cr^{3+} exhibits a distinctive absorption spectrum with a split, broad
396 band centred at 660-700nm attributable to the $A_{2g}(F) \rightarrow {}^4E_{2g}(F)$ transition; and another
397 band with similar intensity occurring at ~450 nm, attributable to the $A_{2g}(F) \rightarrow {}^4E_{1g}(F)$
398 transition [35]. If these recycled cullet/fines or briquettes are reused in glass batch, the
399 compensation of chromium must be set up for the glass colour correction in visible
400 wavelength range.

401 In industrial production, colour and redox state of commercial glasses are usually
402 controlled by the use of oxidizing/ reducing batch constituents, furnace atmosphere
403 and colorants. The redox and colour of glass batches with different amount of
404 briquette studied here was controlled by modification of the manganese ore and
405 chrome premix batch components. In Fig.6b, the absorption spectra of sample
406 Base-line, B-9, B-15 and B-20X are presented. After careful modification, the glasses
407 produced from batches with increasing briquette contents (B-9, B-15 and B-20X)
408 show the same spectral features as the Base line sample and, crucially, the absorption
409 profiles of all samples closely match that of the base line glass, in terms of both
410 spectral profile and quantitatively in terms of absorbance. This is consistent with the
411 colourant (Fe, Cr, Mn) contents of these glasses, which also show no variation within
412 uncertainties of analysis. Consequently, it can be surmised that samples B-9, B-15 and
413 B-20X all have closely similar $\text{Fe}^{2+}/\Sigma\text{Fe}$ redox ratios to the base line glass, and all
414 show low $\text{Fe}^{2+}/\Sigma\text{Fe}$, indicating oxidized glasses. The effects of the manganese ore and
415 chrome premix batch additions were also studied for Series Two glasses, B-15a to
416 B-15d. The main colourant / redox-active components of these raw materials are

417 MnO₂ from manganese ore, and both Cr₂O₃ and Fe₂O₃ from chrome premix. The
418 compositions of B-15a to B-15d are listed in Table 3 and their absorption spectra are
419 shown in Fig.6c. With no manganese ore of chrome premix added, sample B-15a
420 shows the same spectral features as the remelted cullet or remelted glass fines samples
421 in Fig. 6a, which shows that B-15a has a higher Fe²⁺/ΣFe ratio (i.e. more reduced).
422 With insufficient compensation of colorant agents (Manganese ore and Chrome
423 premix), the spectrum characteristic of B-15b between B-15 and B-15a.

424 Manganese in silicate glass normally distributes into Mn²⁺ and Mn³⁺ and
425 generates the absorption band centred at ~500 nm (purple colour) due to Mn³⁺ [36],
426 which undergoes mutual redox interactions with Fe²⁺, thereby reducing to the
427 colourless Mn²⁺ whilst oxidising iron to the weakly yellow/green-coloured Fe³⁺.
428 Small amounts of manganese were introduced because of this oxidising ability. For
429 sample B-15c, the visible absorption spectrum is almost the same as sample B-15.
430 However, due to the absence of Mn ore in the batch for this sample, the broad optical
431 absorption band centered at ~1100 nm (Fe²⁺) is stronger, hence the glass is more
432 reduced and the IR absorption greater. For sample B-15d, the low Cr not only causes
433 the low absorption at 660 - 700 nm and ~450 nm, but also higher absorption at ~1100
434 nm (Fe²⁺).

435

436 **5. Conclusions**

437 Briquettes consisting of 82 wt % recycled glass fines were made with additions of
438 sodium silicate, sodium carbonate and water. Briquette bulk density (2.105 g/cm³) is

439 higher than that of the glass fines (1.311 g/cm^3), as expected. There is faster mass loss
440 ($\sim 0.06 \text{ wt\%/h}$) due to evaporation in the 24 hours following briquette production, and
441 further mass loss due to evaporation is considerably slower ($\sim 0.005 \text{ wt\%/h}$) thereafter.
442 There is also a negative correlation between the initial briquette mass and moisture
443 evaporation rate. The compressive strength of briquettes increases linearly with time,
444 increasing from 2 MPa to 60-65 MPa after 33 days at room temperature (ca. 20°C)
445 and ambient humidity. With compensation of the glass batch materials to maintain a
446 consistent nominal final glass composition, up to 15 wt % briquettes can be added to
447 the batch. These batches rapidly melted to form glasses with comparable properties to
448 briquette-free benchmark glasses. UV-Vis-near IR absorption spectra confirmed that
449 the colour and redox state of resulting glasses can be maintained for different
450 briquette additions. It is thus demonstrated that commercial SLS glasses produced
451 using up to 15 wt% briquetted glass cullet fines exhibit comparable compositions and
452 properties to SLS glasses produced using briquette-free batches, supporting the
453 potential use of this technology for enhanced energy and resource efficiency, and
454 lower CO_2 emissions, from commercial glass manufacture.

455

456 **Acknowledgements**

457 The authors acknowledge financial support from EPSRC under grant EP/P510725/1
458 and Innovate UK under grant 63406-429275. The authors appreciate useful
459 discussions with Vincenzo Starinieri, Francis Clegg, Anthony Bell, Paul Allender, Tim
460 O'Hara and James Burke.

461 Reference

- 462 1. Ruth, M., Dell'Anno, P. An industrial ecology of the US glass industry. *Resources Policy*,
463 1997. **23**(3): p. 109-124.
- 464 2. Hartley, A. A study of the balance between furnace operating parameters and recycled glass in
465 glass melting furnaces. 2004, *Glass Technology Services Ltd*.
- 466 3. Deng, W., et al. Research of Sintering Reactions Process and heat Calculation in Glass batch.
467 *J. Wuhan Univ. Technol.*, 2010. **22**: p. 111-113.
- 468 4. Kovacec M., Pilipovic A., Stefanic N. Impact of glass cullet on the consumption of energy and
469 environment in the production of glass packaging material. *Recent Researches in Chemistry,*
470 *Biology, Environment and Culture. Monteux, Switzerland.* 2011.
- 471 5. Cable, M. A Century of Developments in Glassmelting Research. *J. Am. Chem. Soc.*, 1998.
472 **81**(5): p. 1083-1094.
- 473 6. Schaeffer, H.A. Recycling of cullet and filter dust in the German glass industry.
474 *Glass Sci. Technol.*, 1996. **69**: p. 101-106.
- 475 7. Ross, C.P. Glass Science Tutorial: Lecture #4, Commercial Glass Melting and Associated Air
476 Emission Issues, *U.S. DOE Office*, Editor. Jan. 1995.
- 477 8. Bertuzzi, P., Ercole, P., Ferrero C., Ramon, L. Glassy sand from cullet rejected during primary
478 processing: quality, energy and environmental analysis. in *glass machinery plants &*
479 *accessories* 2009, Smartenergy S.r.l. p. 6.
- 480 9. Hamdan, K.A., Hessenkemper, H., Wiltzsch, S. New Developments of Batch Briquetting, in
481 *74th Conference on Glass Problems*. 2014, *John Wiley & Sons, Inc.* p. 33-42.
- 482 10. Misra, V.N., Reddy, P., Mohapatra, B. Mineral Characterisation and Processing. 2004: *Allied*
483 *Publishers*.
- 484 11. Garkavi, M.S., Kulaeva, N.S. Technological parameters of briquetting batch for foam glass
485 production. *Glass and Ceramics*, 2005. **62**(11): p. 379-380.
- 486 12. Bai, X., Jia, D., Cheng, B.W., Zhao, H.L., Liang, X.P. The influence of the Binders on
487 Compaction of Glass batch. *B. Chin. Ceram. Soc.*, 2009. **28**(3): p. 585-588.
- 488 13. Krashennnikova, N.S., Frolova, I.V., Vereshchagin, V.I. Application of Granulated Raw
489 Concentrate in Glass Technology. *Glass and Ceramics*, 2004. **61**(5): p. 164-167.
- 490 14. Beerkens, R., Energy saving options for glass furnaces & recovery of heat from their flue
491 gases and experiences with batch & cullet pre-heaters applied in the glass industry. in *69th*
492 *Conference on Glass Problems: Ceramic Engineering and Science Proceedings*, C.H.
493 Drummond, Editor. 2009, John Wiley & Sons, Inc.: Hoboken, NJ, USA. .
- 494 15. Simpson, W., Myers, D. The Redox Number Concept and Its Use by the Glass Technologist.
495 *Glass Technol.*, 1978. **19**: p. 82-85.
- 496 16. Goldman, D.S., Oxidation Equilibrium of Iron in Borosilicate Glass. *J. Am. Chem. Soc.*, 1983.
497 **66**(3): p. 205-209.
- 498 17. Shi, X.Y., Brungs, M.P., Young, D.J. The iron redox couple and its interaction with sulphur in
499 glass. *Phys. Chem. Glasses*, 1995. **36**(6): p. 275-278.
- 500 18. Beerkens, R. Amber chromophore formation in sulphur- and iron-containing soda-lime-silica
501 glasses. *Glass Sci. Technol.* 2003. **76**(4): p. 166-175.
- 502 19. Shelby, J.E., Introduction to Glass Science and Technology. 2005: *Royal Society of Chemistry*.
- 503 20. Kröger, C., Eligehausen. H. *Über das Wärmeleitvermögen des einschmelzenden*

- 504 *Glasgemenges. Glastechn. Ber.*, 1959. **9**(32): p. 362-373.
- 505 21. Verheijen, O., Beerkens, R., Op den Camp. O. Thermal heat conductivity of glass forming
506 batches. in *Glass Odyssey: Proc. Sixth ESG Conf.* 2002.
- 507 22. Schill, P., Lutze, W. Modeling the behavior of noble metals during HLW vitrification in the
508 DM1200 melter, *VSL-05R5740-1*, Vitreous State Laboratory, Washington DC, 2005.
- 509 23. Pokorny, R., et al. Determination of temperature-dependent heat conductivity and thermal
510 diffusivity of waste glass melter feed. *J. Am. Chem. Soc.*, 2013. **96**(6): p. 1891-1898.
- 511 24. Wang, J., et al. Melting properties of loose and granulated glass batch. *J. Wuhan Univ.*
512 *Technol.-Mater. Sci. Ed.*, 2014. **29**(6): p. 1161-1164.
- 513 25. Faber, A.J., Beerkens, R., Waal, H.d. Thermal behaviour of glass batch on batch heating.
514 *Glustech. Ber.*, 1992. **65**(7): p. 177-185.
- 515 26. Parappagoudar, M., Pratihari, D., Datta, G. Neural network-based approaches for forward and
516 reverse mappings of sodium silicate-bonded, carbon dioxide gas hardened moulding sand
517 system. *Materials and Manufacturing Processes*, 2008. **24**(1): p. 59-67.
- 518 27. Owusu, Y.A. Physical-chemistry study of sodium silicate as a foundry sand binder. *Adv.*
519 *Colloid Interface Sci.*, 1982. **18**(1): p. 57-91.
- 520 28. Chang, C.F., Chen J.W. The experimental investigation of concrete carbonation depth. *Cem.*
521 *Concr. Res.*, 2006. **36**(9): p. 1760-1767.
- 522 29. Paul, A., Oxidation — Reduction Equilibrium in Glass Forming Melts, in Amorphous
523 Magnetism II, *R.A. Levy and R. Hasegawa, Editors.* 1977, Springer US: Boston, MA. p.
524 597-611.
- 525 30. Bingham, P.A. The environment of iron in silicate glasses, in *Materials Science and*
526 *Engineering.* 2001, University of Sheffield.
- 527 31. Wright, A.C., Clarke, S.J., Howard, C.K., Bingham, P.A., et al. The environment of
528 Fe²⁺/Fe³⁺ cations in a soda-lime-silica glass. *Physics and Chemistry of Glasses : European*
529 *Journal of Glass Science and Technology Part B*, 2014. **55**(6): p. 243-252.
- 530 32. Bingham, P.A., et al. Redox and clustering of iron in silicate glasses. *J. Non-Cryst. Solids*,
531 1999. **253**(1-3): p. 203-209.
- 532 33. Volotinen, T.T. Mathematical description of absorbance spectra fo Fe and Cu doped
533 soda-line-silica glasses, in *The Department of Engineering materials.* 2007, The University of
534 Sheffield.
- 535 34. Bingham, P.A., et al., Novel structural behaviour of iron in alkali-alkaline-earth-silica glasses.
536 *Comptes Rendus Chimie*, 2002. **5**(11): p. 787-796.
- 537 35. Bingham, P.A, Connelly, A.J., Hand, R.J., Hyatt, N.C., Northrup, P.A., Alonso Mori, R.,
538 Glatzel, P., Kavcic, M., Zitnik, M., Bucar, K., Edge, R. A multi-spectroscopic investigation of
539 sulphur speciation in silicate glasses and slags. *Glass Technol.*, 2010. **51**(2): p. 63-80.
- 540 36. Thiemsorn, W., et al., Redox ratio and optical absorption of polyvalent ions in industrial
541 glasses. *Bull. Mater. Sci.*, 2007. **30**(5): p. 487-495.
- 542

Table 1. Batch compositions of sample glasses

a)

	Baseline Wt %	B-9 Wt %	B-15 Wt %	B-20X Wt %
Other ingredients (sand, limestone, dolomite etc.)	12.53	11.37	10.63	10.35
Cullet	87.47	79.54	74.47	69.75
Briquette	0	9.09	14.9	19.9
SUM	100	100	100	100

b)

	B-15a Wt %	B-15b Wt %	B-15c Wt %	B-15d Wt %
	No colorant	No colorant for briquette	No Mn	No Cr
Other ingredients	9.51	9.51	9.51	9.51
Chrome premix	0	0.81	0.94	/
Manganese ore	0	0.15	/	0.18
Cullet	74.47	74.47	74.47	74.47
Briquette	14.9	14.9	14.9	14.9
SUM	98.88	99.84	99.82	99.06

Table 2. Bulk and true densities of container glass, glass fine and briquette.

	Container glass	Glass fines	Briquette
Bulk density (g/cm ³)	2.544	1.311	2.105
True density (g/cm ³)	2.544	2.513	n/m *

* The true density of briquette cannot be measured as the binder is water soluble.

Table 3. a) Series One XRF analysed glass compositions in wt % (the nominal composition of B-9, 15, 20x should be the same as Base line)

	Baseline	B-9	B-15	B-20X	Cullet	Glass fines	Briquettes
Na ₂ O	13.24	13.63	13.53	14.71	13.64	13.18	16.54
MgO	1.97	1.85	1.98	1.91	1.31	1.84	1.76
Al ₂ O ₃	2.78	2.89	2.85	2.71	2.99	2.57	1.73
SiO ₂	69.53	69.58	70.09	69.01	71.09	71.56	69.18
K ₂ O	1.10	0.88	0.85	0.81	0.82	0.89	0.72
CaO	9.92	9.63	9.32	9.34	9.31	9.13	9.48
Cr ₂ O ₃	0.38	0.39	0.38	0.39	0.10	0.10	0.12
MnO	0.18	0.19	0.18	0.19	0.07	0.05	\
Fe ₂ O ₃	0.57	0.59	0.53	0.57	0.40	0.34	0.34
SO ₃	0.09	0.17	0.08	0.12	0.06	0.04	0.04
P ₂ O ₅	\	\	\	\	0.03	0.03	\
TiO ₂	0.09	\	\	\	\	0.07	\
SrO	0.08	0.10	0.10	0.10	0.02	0.03	\
BaO	0.07	0.07	0.07	0.08	0.10	0.13	0.07
Cl	\	0.03	0.04	0.06	0.03	\	\
PbO	\	\	\	\	\	0.04	0.02
SUM	100	100	100	100	100	100	100

Table 3. b) Series Two XRF analysed glass compositions in wt %

	B-15a	B-15b	B-15c	B-15d
Na ₂ O	13.54	13.46	13.51	13.45
MgO	1.87	1.87	1.86	1.84
Al ₂ O ₃	3.19	3.18	3.13	3.14
SiO ₂	70.12	70.05	70.00	70.20
K ₂ O	0.87	0.86	0.83	0.87
CaO	9.39	9.36	9.32	9.27
Cr ₂ O ₃	0.11	0.23	0.37	0.15
MnO	0.06	0.14	0.07	0.19
Fe ₂ O ₃	0.48	0.49	0.50	0.48
SO ₃	0.09	0.09	0.10	0.09
P ₂ O ₅	\	\	\	\
TiO ₂	0.07	0.07	0.07	0.07
SrO	0.09	0.08	0.08	0.10
BaO	0.07	0.08	0.09	0.09
Cl	0.03	0.02	0.04	0.03
PbO	0.02	0.02	0.03	0.03
TOTAL	100	100	100	100

Figure 1. Analyzed particle size distribution of glass fines

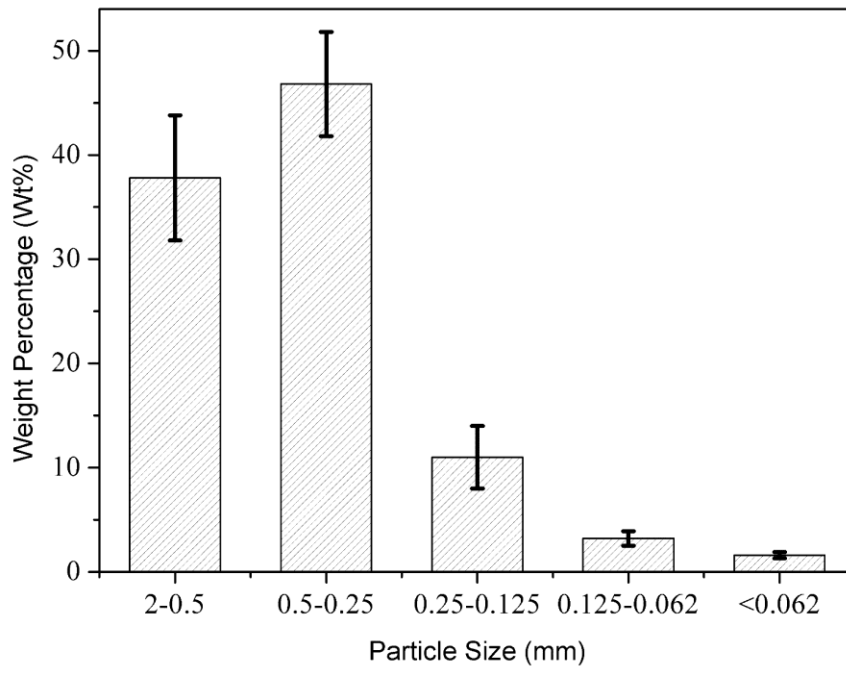




Figure 2. a) Optical micrographs of recycled glass fines; b) Optical micrographs of recycled glass fines washed by acetone in ultrasonic bath for 2mins and then dried.

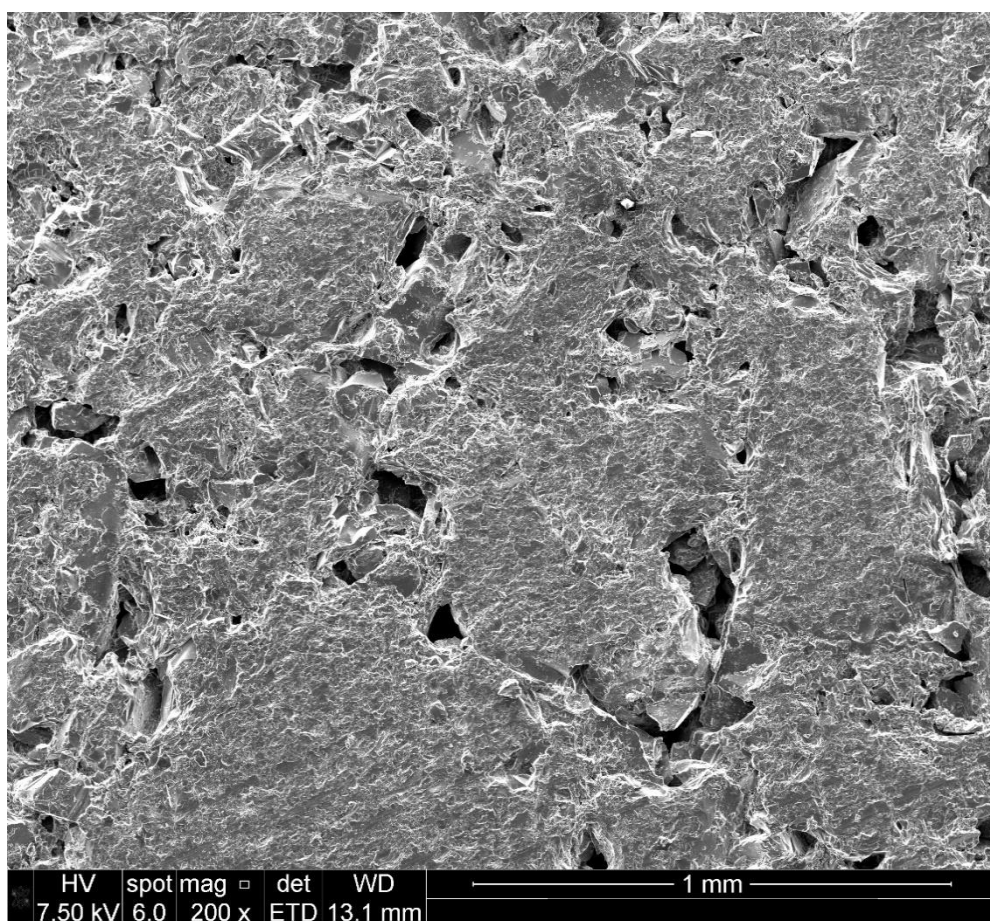
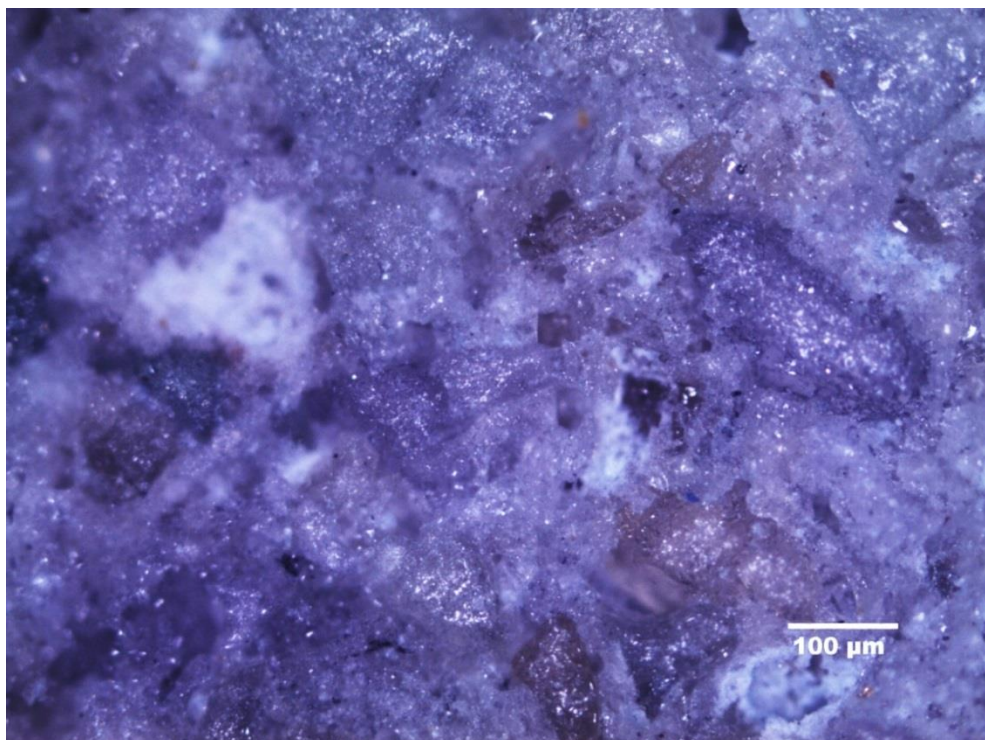


Figure 3.a) Optical and b) Secondary electron SEM images of briquette surface x 200.

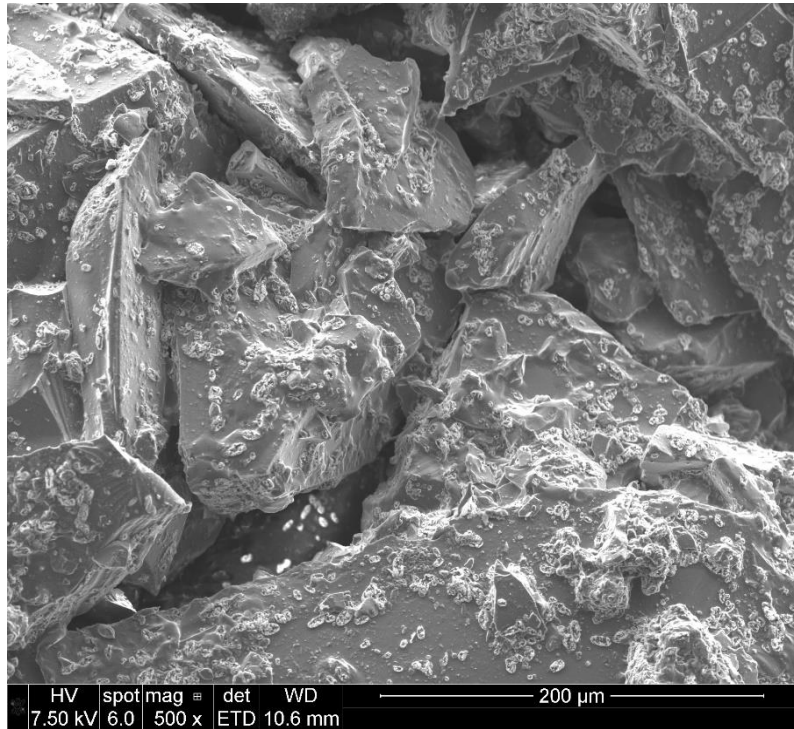
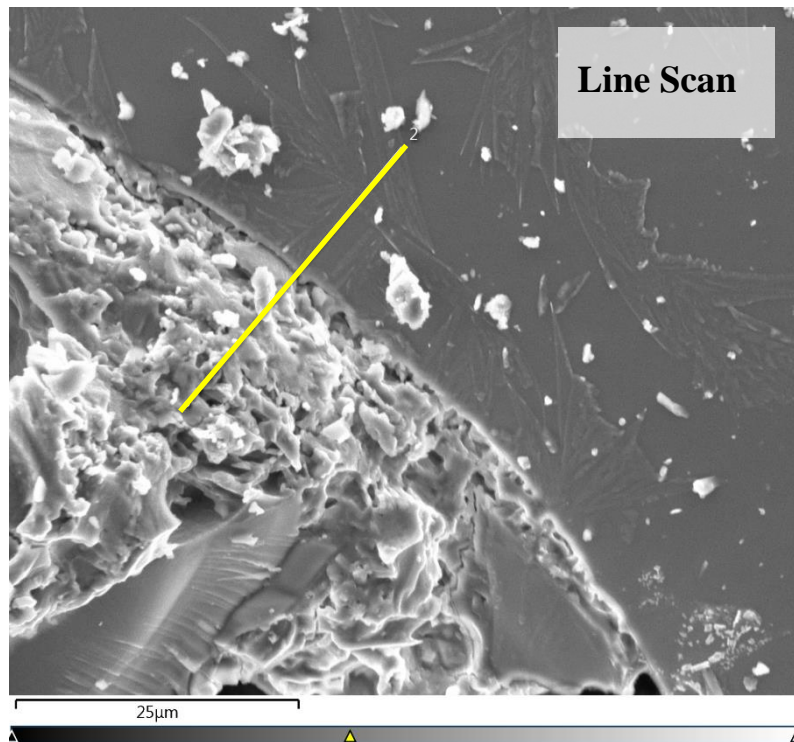


Figure 3.c) Secondary electron SEM image of briquette cross-section x 500.



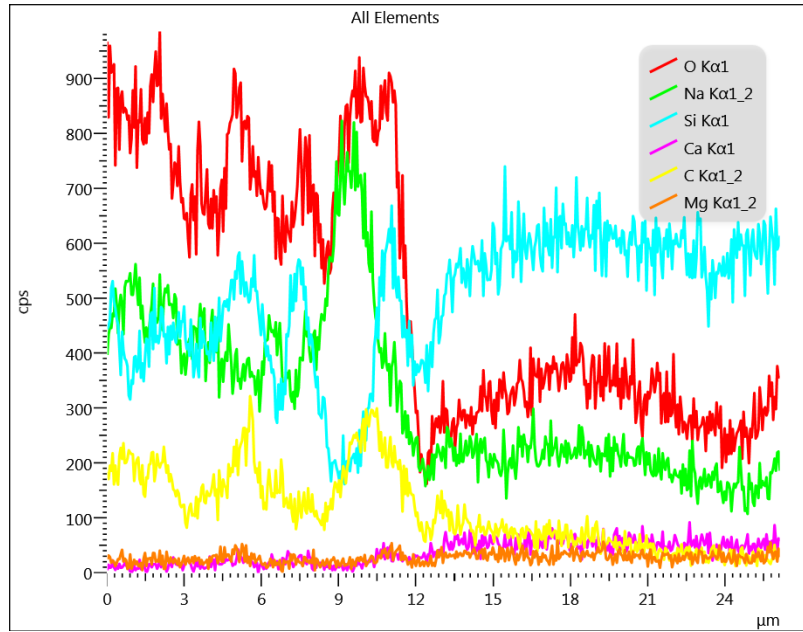
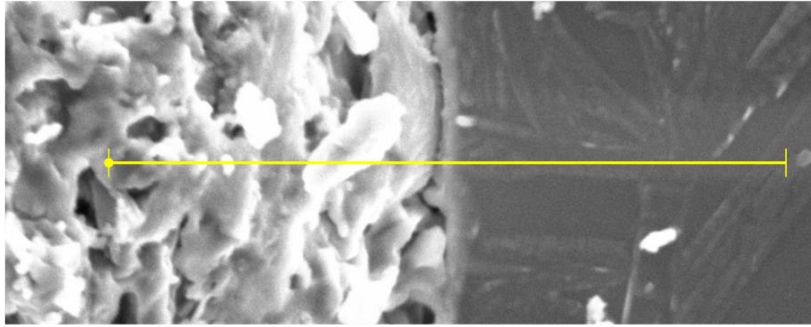


Figure 3.d) EDS line scan result of continuous phase / glass particle interface in briquette.

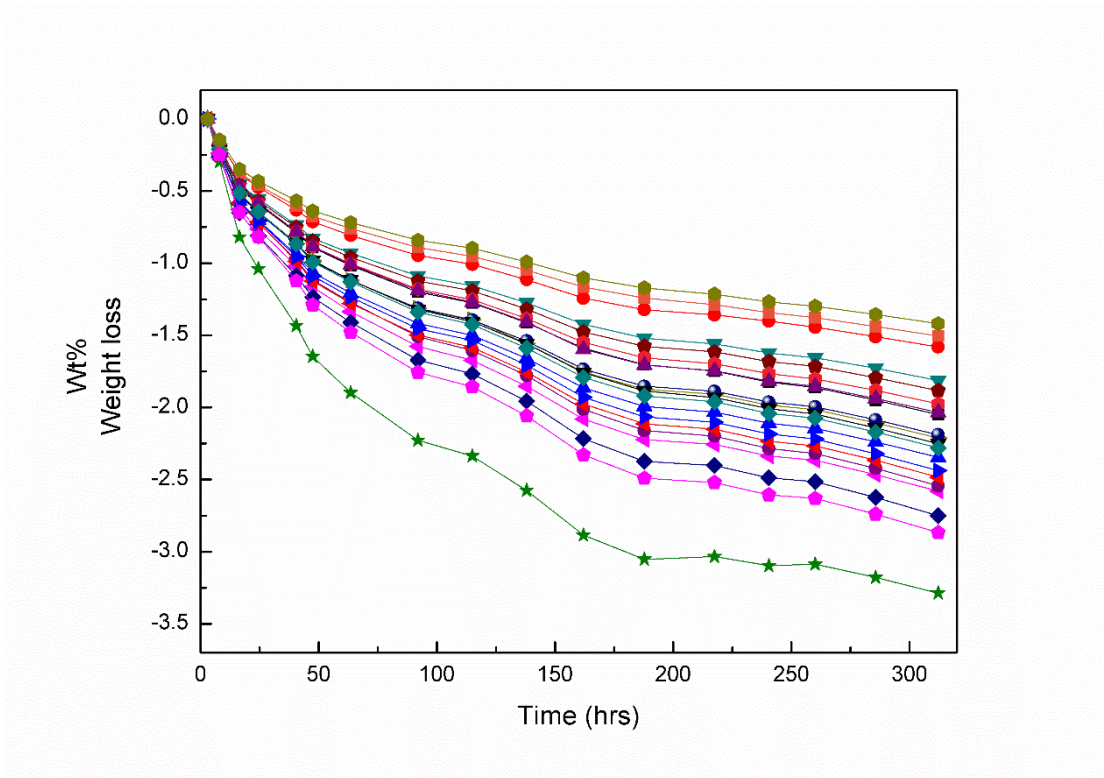


Figure 4. Briquette weight loss as *fn.* (time after forming) for 20 briquettes at room temperature.

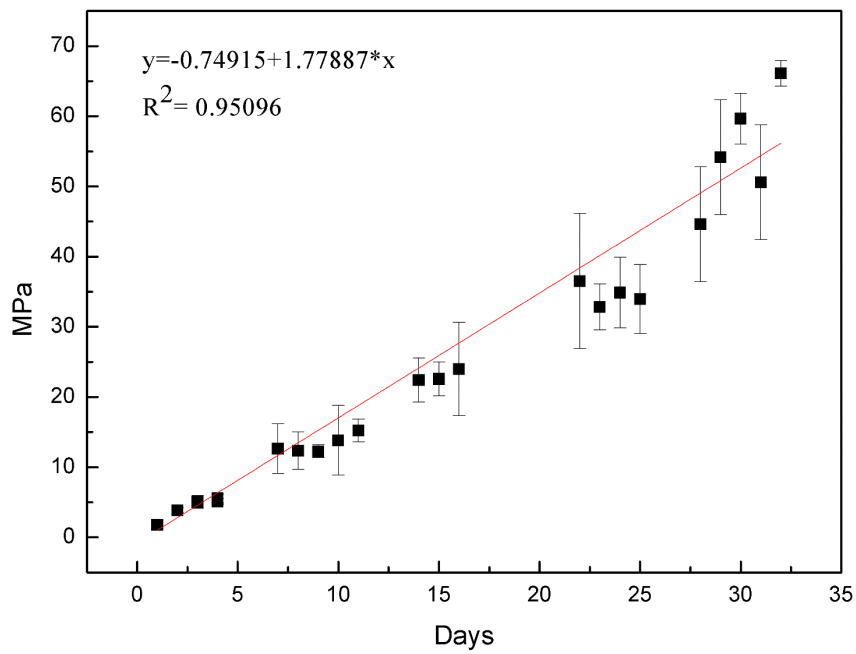


Figure 5. Compressive strength of briquettes as *fn.*, line shown as visual guide (time after forming).

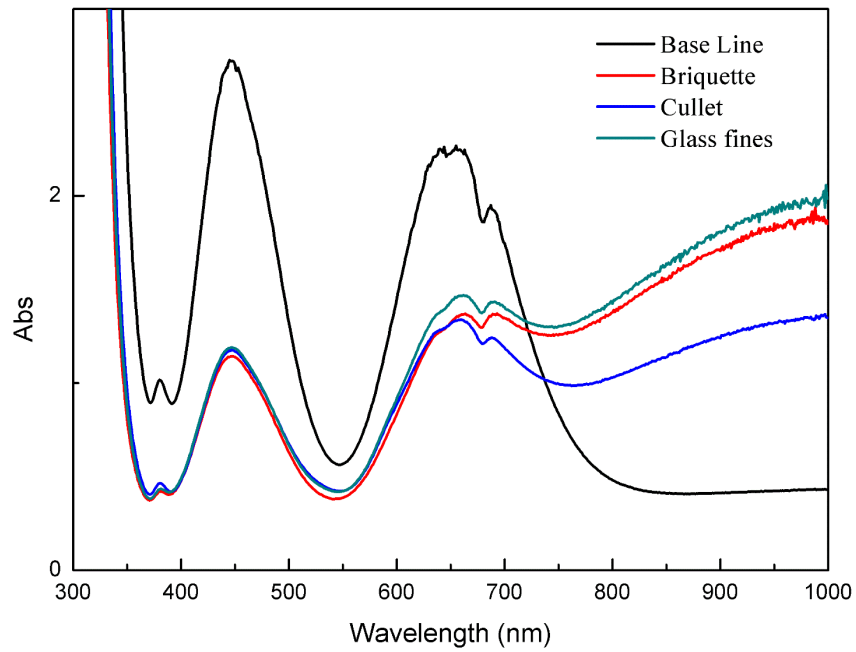


Fig.6 a) UV-Vis-Near IR absorption spectra of baseline, melted briquette, melted cullet and melted glass fines samples.

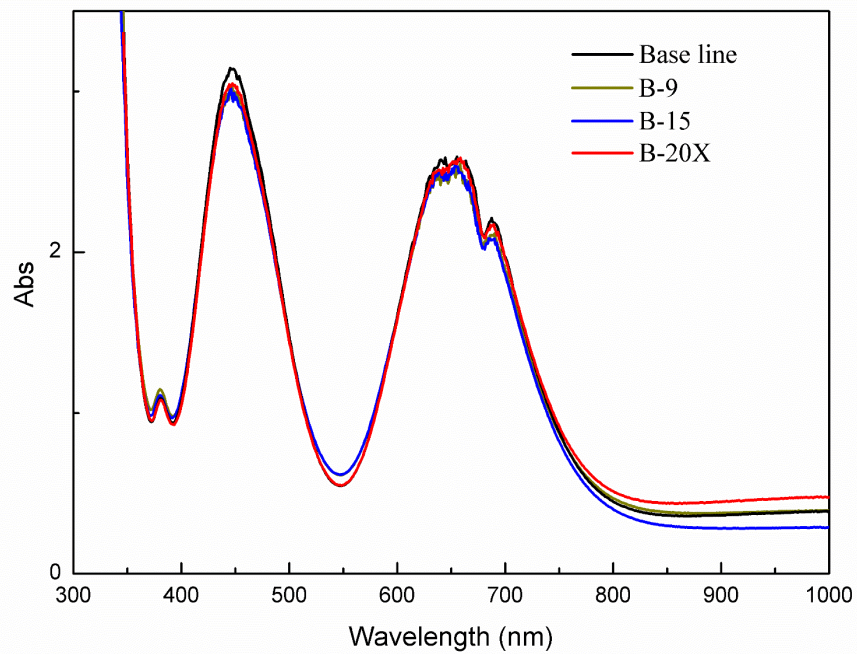


Fig.6 b) UV-Vis-Near IR absorption spectra of samples baseline, B-9, B-15 and B-20X.

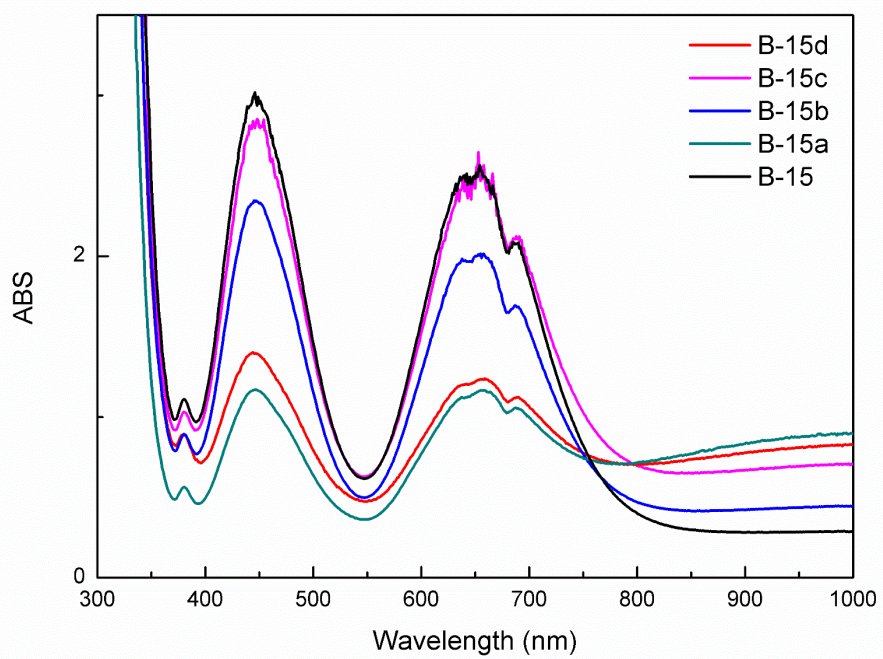


Fig.6 c) UV-Vis-Near IR absorption spectra of samples B-15, B-15a, B-15b, B-15c and B-15d.

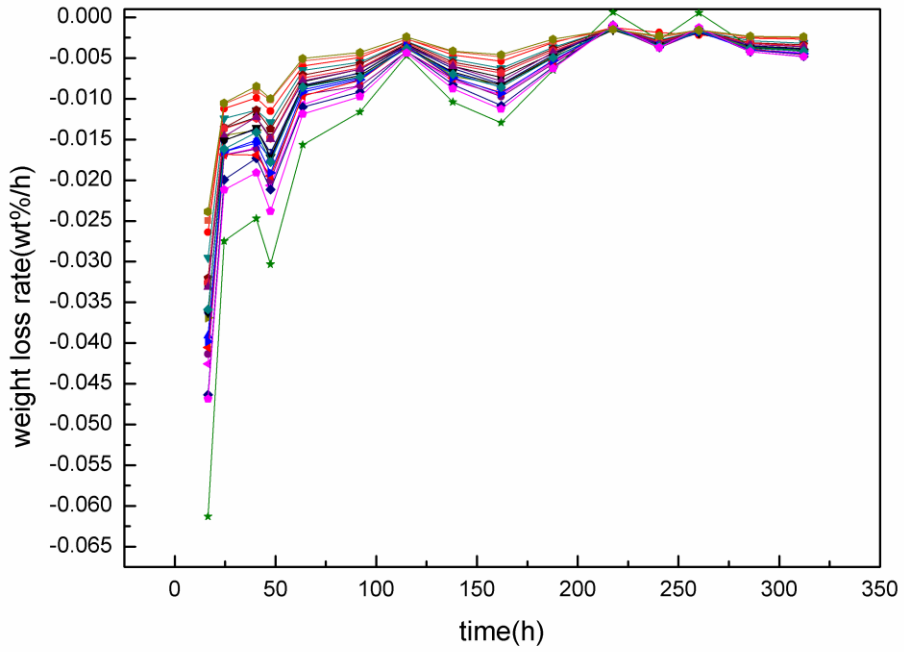


Fig.7 a) Weight loss rates for different briquettes as *fn.* (time) at 20 °C.

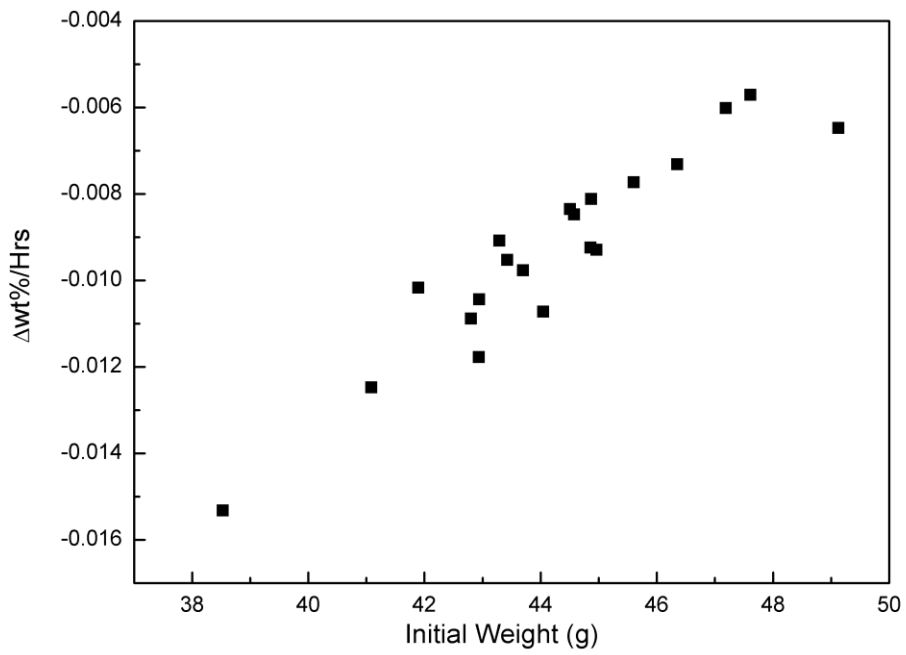


Fig.7 b) Average weight loss rate of 20 briquettes after 187 hours vs. initial weight of briquettes.

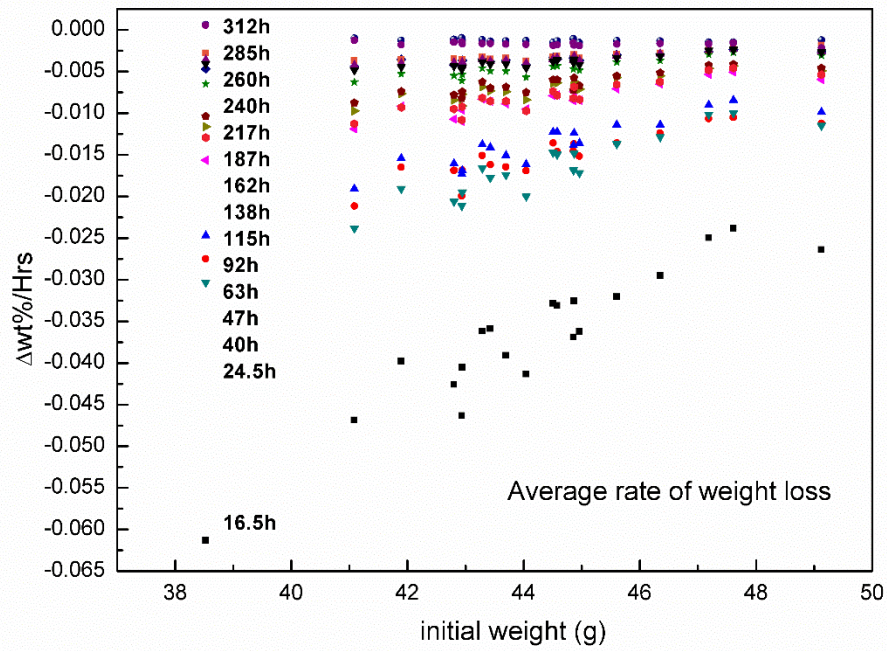


Fig.7 c) Average weight loss rate of 20 briquettes in different time vs. initial weight of briquettes.